Primary-side Voltage Control for High-efficiency Operation of Wireless High-precision Stage

Takumi Hayashi* Student Member, Hiroshi Fujimoto* Senior Member
Koichi Sakata** Senior Member, Zhaoxiang Chen** Non-member

High-precision stages in lithography systems are crucial for manufacturing flat panel displays and semiconductors. The wireless high-precision stage (WHPS) has been developed, which employs wireless power transfer (WPT) instead of power cables to address the issues caused by power cables of the conventional stages. The aim of this study is to develop a high-efficiency operation method of WHPS for its practical application. In the proposed approach, the primary-side voltage is designed based on the secondary-side rectification ratio under the two-mode control to stabilize the WPT system. Simulations and experiments are performed, and the effectiveness of the proposed approach is demonstrated.

Keywords: High-precision stage, wireless high-precision stage, wireless power transfer, high-efficiency operation.

1. Introduction

High-precision stages in lithography systems play an important role in manufacturing flat panel displays and semiconductors. High-speed and high-precision positioning of the stages is pursued for high-throughput and high-quality manufacturing. Both software and hardware approaches have been developed to enhance control performance. High-performance inversion-based feedforward control[(1),(2)] and data-driven feedback controller design[(3)] are the software approaches, while new stage structures[(4),(5)] have been proposed as the hardware approaches. Recent progress is summarized in the references.[(6)–(8)]

In the high-precision stages, contactless actuators such as linear motors and contactless guides such as air guides are widely used to suppress floor vibration and friction. The remaining issue is the problem caused by cables. Power cables for the power supply of actuators and sensors, communication lines, and pneumatic pipes for the air guide are all connected. These cables cause cable tension disturbance and contamination, and thus degrade the control performance of the stages. To address the issues caused by the cables, our research group has developed the wireless high-precision stage (WHPS),[(9)] which is the stage driven by wireless power transfer (WPT) instead of the power cables.

WHPS has successfully reduced the problems caused by power cables.[(10)] The remaining issue of WHPS is power transmission efficiency. The power transmission loss leads to heat loss. Generally, high-precision stages are operated under strict temperature management because temperature variation in lithography systems causes mechanical deformation and variation in optical properties of lithography systems.[(11)] Therefore, high-efficiency operation of WHPS is required for its industrial application.

The optimal voltage ratio method[(12)] is often used to improve the power transmission efficiency of WPT systems. In this method, the AC-AC power transmission efficiency of the WPT system is maximized by setting the ratio between the primary-side and secondary-side voltage to the optimal value. However, the WPT system of WHPS is stabilized by the two-mode control method, which switches the rectification and short modes of the secondary-side rectifier. In this case, the optimal voltage ratio cannot reduce the power transmission loss because it does not consider the mode switching. On the other hand, the primary-side voltage control method considering the mode switching has been proposed, named the short-mode loss reduction method.[(13)] The latter approach, however, does not consider AC-AC power transmission efficiency.

The aim of this study is to develop a high-efficiency power transmission method considering both the AC-AC power transmission efficiency and the mode switching of the two-mode control method. In the proposed approach, the rectification ratio is focused on, and high-efficiency power transmission is achieved by balancing the above two conventional methods. The contributions of this study are summarized as follows:

- The primary-side voltage control for high-efficiency operation of WHPS is proposed.
- The presented approach is compared with the conventional approaches.
- The effectiveness of the presented approach is verified through simulations and experiments with WHPS.

The remainder of this paper is organized as follows. In Section 2, the experimental setup, WHPS, is presented. Then, Section 3 introduces the conventional approaches for high-efficiency operation of WHPS. In addition, the disadvantages of the conventional approaches are summarized. Next, in

* The University of Tokyo
5-1-5, Kashiwanoha, Kashiwa, Chiba, Japan
** Nikon Corporation
47-1, Nagaodaicho, Sakae, Yokohama, Kanagawa, Japan

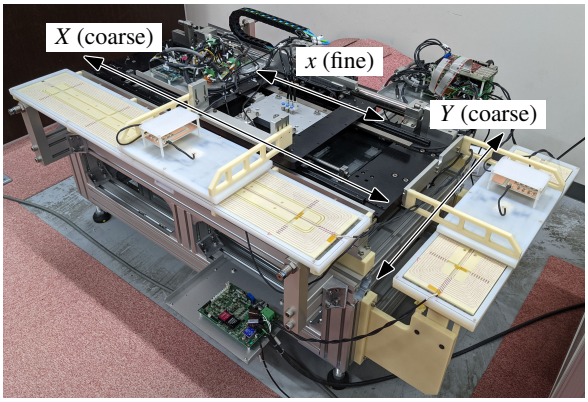

Fig. 1. Picture of WHPS.

Table 1. Circuit parameters of WHPS.

Symbol	Definition	Value
f_0	Operating frequency	85 kHz
L_1	Primary-side self-inductance	108 µH
C_1	Primary-side capacitance	33.6 nF
R_1	Primary-side resistance	687 mΩ
L_2	Secondary-side self-inductance	47.6 µH
C_2	Secondary-side capacitance	76.0 nF
R_2	Secondary-side resistance	264 mΩ
L_m	Mutual inductance	25 µH
C_s	Secondary-side smoothing capacitance	1000 µF

Section 4, the proposed approach for high-efficiency operation of WHPS is presented. The proposed approach is validated through simulations and experiments in Section 5. Finally, Section 6 concludes this paper.

2. Wireless High-precision Stage

In this section, the experimental setup, WHPS, is introduced. Furthermore, the WPT system of WHPS and its stabilization method is described.

2.1 Structure of WHPS The picture of WHPS is shown in Fig. 1. WHPS has the two-axis coarse stage (X and Y axis) and the single-axis fine stage (x axis). The X and Y axis coarse stages are driven by the linear motors, and the x axis fine stage is driven by the voice coil motor. Each axis is guided by the air guide to reduce the effect of friction. In this study, only the X axis coarse stage is used. The DC voltage source is directly connected to the primary side of the WPT system of the X axis coarse stage.

2.2 WPT system of WHPS The series-series (S-S) compensated WPT system is employed to achieve high efficiency in WHPS. Fig. 2 shows the system configuration of the X axis coarse stage. Here, L, C, and R are the self-inductance, capacitance, and resistance, respectively. The subscript 1 and 2 denote the primary and secondary sides. L_m is the mutual inductance and C_s is the smoothing capacitance. These values are summarized in Table 1.

A rectangular wave of the operating frequency f_0 is generated from the DC voltage source V_{in} by the primary-side inverter. Next, the power is wirelessly transferred from the primary to the secondary sides. Then, the AC voltage is converted to DC voltage V_L by the secondary-side rectifier and the smoothing capacitor. Finally, the DC voltage is applied to the motor driver, and the linear motor is driven.

2.3 Secondary-side Voltage Stabilization The WPT system of WHPS is connected to the linear motor, one of the constant power loads. This type of WPT system is unstable, and the secondary-side voltage diverges.[14] To stabilize the WPT system, the two-mode control method using the hysteresis comparator is currently implemented in WHPS.

The two-mode control method is illustrated in Fig. 3. If the receiving power of the secondary side is larger than the load power, the secondary-side DC voltage increases in the rectification mode, while it decreases in the short mode. By switching these two modes, the secondary-side DC voltage is stabilized and kept within a certain range.

3. Conventional Approach for High-efficiency Operation of WHPS

In this section, two conventional approaches for high-efficiency operation of WHPS are presented. One is based on the optimal voltage ratio between the primary and secondary sides,[12] and the other is reducing the short-mode loss of the secondary side.[13]

3.1 Optimal Voltage Ratio Method First, the optimal voltage ratio between the primary and secondary sides is derived, which maximizes the transmission efficiency of AC-AC power.[12]

Fig. 4 shows the equivalent circuit of the WPT system. In this circuit, the following resonance condition is assumed to hold:

$$\omega_0 = 2\pi f_0 = \frac{1}{\sqrt{L_1 C_1}} = \frac{1}{\sqrt{L_2 C_2}}, \quad \cdots\cdots (1)$$

where ω_0 is the operating angular frequency.

The primary-side and secondary-side current are derived from Kirchhoff's voltage law as follows:

$$I_1 = \frac{R_2 V_1 + \omega_0 L_m V_2}{R_1 R_2 + (\omega_0 L_m)^2}, \quad \cdots\cdots (2)$$

$$I_2 = \frac{\omega_0 L_m V_1 - R_1 V_2}{R_1 R_2 + (\omega_0 L_m)^2}. \quad \cdots\cdots (3)$$

Here, $V_{1/2}$ and $I_{1/2}$ denote the effective values of $v_{1/2}$ and $i_{1/2}$. Therefore, the transmission and receiving power, P_1 and P_2, are given by

$$P_1 = \frac{R_2 V_1^2 + \omega_0 L_m V_1 V_2}{R_1 R_2 + (\omega_0 L_m)^2}, \quad \cdots\cdots (4)$$

$$P_2 = \frac{\omega_0 L_m V_1 V_2 - R_1 V_2^2}{R_1 R_2 + (\omega_0 L_m)^2}. \quad \cdots\cdots (5)$$

According to (4) and (5), the AC-AC power transmission efficiency, $\eta_{ac} = P_2/P_1$, is calculated as

$$\eta_{ac} = \frac{\omega_0 L_m V_1 V_2 - R_1 V_2^2}{\omega_0 L_m V_1 V_2 + R_2 V_1^2}. \quad \cdots\cdots (6)$$

By taking the derivative of η_{ac} with respect to the voltage ratio $A_v = V_2/V_1$, the optimal voltage ratio A_{vopt} which maximizes η_{ac} is derived as follows:

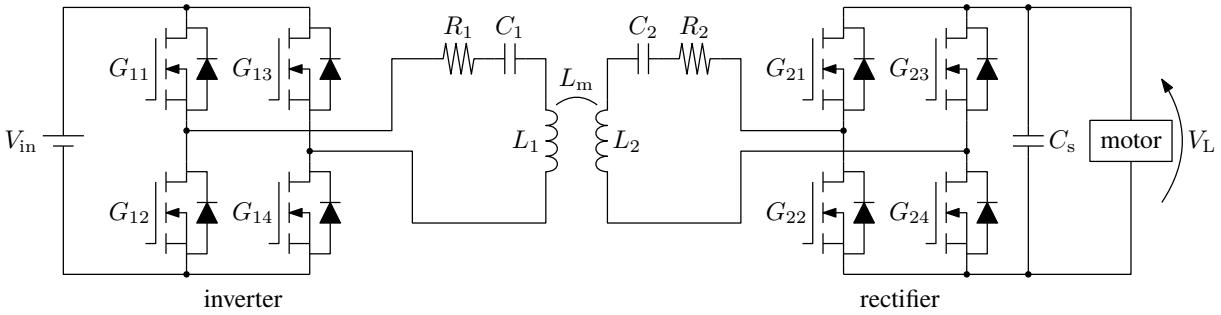

Fig. 2. System configuration of WHPS.

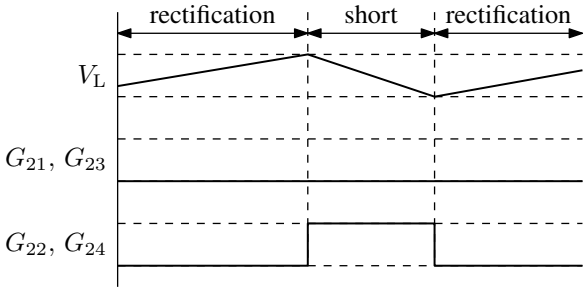

Fig. 3. Two-mode control method.

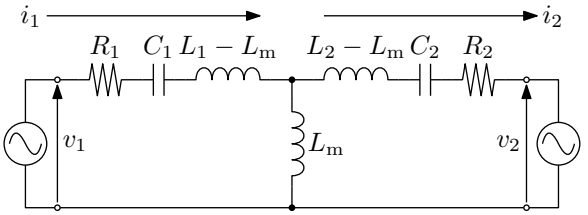

Fig. 4. Equivalent circuit of S-S WPT system.

$$A_{\rm vopt} = \sqrt{\frac{R_2}{R_1}} \frac{\omega_0 L_{\rm m}}{\sqrt{R_1R_2 + (\omega_0 L_{\rm m})^2} + \sqrt{R_1R_2}}. \cdots\cdots (7)$$

Finally, the primary-side voltage V_1 is designed as follows:

$$V_1 = \frac{V_2}{A_{\rm vopt}}. \cdots\cdots (8)$$

Here, the secondary-side voltage V_2 is assumed to be predetermined.

3.2 Short-mode Loss Reduction Method Next, the short-mode loss reduction method[13] is described.

Under the two-mode control, the rectification and short modes are repeated to stabilize the WPT system. The secondary-side voltage V_2 in the rectification and short modes, $V_{2\rm r}$ and $V_{2\rm s}$ is given by

$$V_{2\rm r} = \frac{2\sqrt{2}}{\pi} V_{\rm L}, \cdots\cdots (9)$$
$$V_{2\rm s} = 0. \cdots\cdots (10)$$

Then, the transmission power in the rectification and short modes, $P_{1\rm r}$ and $P_{1\rm s}$, is derived from (4) as follows:

$$P_{1\rm r} = \frac{R_2 V_1^2 + \frac{2\sqrt{2}}{\pi}\omega_0 L_{\rm m} V_1 V_{\rm L}}{R_1R_2 + (\omega_0 L_{\rm m})^2}, \cdots\cdots (11)$$
$$P_{1\rm s} = \frac{R_2 V_1^2}{R_1R_2 + (\omega_0 L_{\rm m})^2}. \cdots\cdots (12)$$

Furthermore, according to (5), the receiving power in the rectification and short modes, $P_{2\rm r}$ and $P_{2\rm s}$, is given by

$$P_{2\rm r} = \frac{\frac{2\sqrt{2}}{\pi}\omega_0 L_{\rm m} V_1 V_{\rm L} - \frac{8}{\pi^2} R_1 V_{\rm L}^2}{R_1R_2 + (\omega_0 L_{\rm m})^2}, \cdots\cdots (13)$$
$$P_{2\rm s} = 0. \cdots\cdots (14)$$

(12) and (14) indicate that the power transmission in the short mode results in a loss. It is, therefore, expected that high-efficiency power transmission is achieved by reducing the short mode. By solving $P_{2r} = P_{\rm L}$ where $P_{\rm L}$ is the load power, the primary-side voltage which minimizes the short-mode loss is derived as

$$V_1 = \frac{2\sqrt{2}}{\pi}\frac{R_1 V_{\rm L}}{\omega_0 L_{\rm m}} + \frac{\pi}{2\sqrt{2}}\frac{\left\{R_1R_2 + (\omega_0 L_{\rm m})^2\right\} P_{\rm L}}{\omega_0 L_{\rm m} V_{\rm L}}. \cdots (15)$$

3.3 Disadvantage of Conventional Approach The disadvantages of the above two approaches are presented.

The optimal voltage ratio method maximizes the AC-AC power transmission efficiency. The short-mode loss, however, is not considered. It becomes large, especially when the secondary-side voltage is fixed and the load power is relatively small.

On the other hand, the latter approach reduces the short-mode loss by designing the primary-side voltage based on the load power. The AC-AC power transmission efficiency, however, is not considered. In addition, the WPT system easily diverges due to the transmission power shortage caused by some reasons, e.g., measurement errors of the circuit parameters and loss in the secondary-side rectifier. For these reasons, the short-mode loss reduction method is difficult to implement practically.

4. Proposed Approach for High-efficiency Operation of WHPS

In this section, the proposed approach for high-efficiency operation of WHPS is presented. The aim of the proposed approach is to reduce the total transmission power (and energy) by balancing the two conventional approaches. The approach is based on the rectification ratio introduced in this section.

First, the rectification ratio α is defined as follows:

$$\alpha = \frac{T_{\rm r}}{T_{\rm r} + T_{\rm s}}, \cdots\cdots (16)$$

where $T_{\rm r}$ and $T_{\rm s}$ are the rectification-mode and short-mode time of the two-mode control.

Then, the average output current of the secondary-side rectifier under the two-mode control, $\bar{I}_{\rm s}$, is given by

$$\overline{I}_{\mathrm{s}} = \frac{2\sqrt{2}}{\pi} I_2 \alpha \quad \cdots\cdots (17)$$

$$= \frac{2\sqrt{2}}{\pi} \frac{\omega_0 L_{\mathrm{m}} V_1 - \frac{2\sqrt{2}}{\pi} R_1 V_{\mathrm{L}}}{R_1 R_2 + (\omega_0 L_{\mathrm{m}})^2} \alpha \quad \cdots\cdots (18)$$

$$= \frac{P_{\mathrm{L}}}{V_{\mathrm{L}}}. \quad \cdots\cdots (19)$$

The rectification ratio α, therefore, is derived from (18) and (19) as follows:

$$\alpha = \frac{\pi}{2\sqrt{2}} \frac{R_1 R_2 + (\omega_0 L_{\mathrm{m}})^2}{\omega_0 L_{\mathrm{m}} V_1 - \frac{2\sqrt{2}}{\pi} R_1 V_{\mathrm{L}}} \frac{P_{\mathrm{L}}}{V_{\mathrm{L}}}. \quad \cdots\cdots (20)$$

Futhermore, when the rectification ratio is α, the primary-side voltage $V_1(\alpha)$ is represented as

$$V_1(\alpha) = \frac{2\sqrt{2}}{\pi} \frac{R_1 V_{\mathrm{L}}}{\omega_0 L_{\mathrm{m}}} + \frac{\pi}{2\sqrt{2}} \frac{\left\{R_1 R_2 + (\omega_0 L_{\mathrm{m}})^2\right\} P_{\mathrm{L}}}{\alpha \omega_0 L_{\mathrm{m}} V_{\mathrm{L}}}. \quad (21)$$

When the rectification ratio is α, the average transmission power under the two-mode control, $\overline{P}_1(\alpha)$, is calculated from (11), (12), and (21) as follows:

$$\overline{P}_1(\alpha) = \frac{R_2 (V_1(\alpha))^2 + \frac{2\sqrt{2}}{\pi} \alpha \omega_0 L_{\mathrm{m}} V_1(\alpha) V_{\mathrm{L}}}{R_1 R_2 + (\omega_0 L_{\mathrm{m}})^2}. \quad \cdots\cdots (22)$$

Then, the average power transmission efficiency under the two-mode control, $\overline{\eta}(\alpha)$, is given by

$$\overline{\eta}(\alpha) = \frac{R_1 R_2 + (\omega_0 L_{\mathrm{m}})^2}{R_2 (V_1(\alpha))^2 + \frac{2\sqrt{2}}{\pi} \alpha \omega_0 L_{\mathrm{m}} V_1(\alpha) V_{\mathrm{L}}} P_{\mathrm{L}}. \quad \cdots\cdots (23)$$

In the proposed approach, the reference of the rectification ratio is selected to maximize the average power transmission efficiency, i.e.,

$$r_\alpha = \alpha_{\mathrm{opt}}, \quad \cdots\cdots (24)$$

$$\alpha_{\mathrm{opt}} = \arg\max_{0<\alpha\leq 1} \overline{\eta}(\alpha), \quad \cdots\cdots (25)$$

where r_α and α_{opt} are the reference of the rectification ratio and the optimal rectification ratio. Then, the primary-side voltage V_1 is designed base on (21). The proposed approach considers both the AC-AC power transfer efficiency and the short-mode loss. Note that the short-mode loss reduction method is recovered from the proposed approach as a special case if $r_\alpha = 1$.

5. Validation

In this section, the proposed approach for high-efficiency operation of WHPS is validated through simulations and experiments.

5.1 Target Operation The operation of WHPS considered in this section is presented in Fig. 5. The position reference shown in Fig. 5(a) is a trapezoidal trajectory consisting of acceleration, constant velocity, and deceleration period. The stage is driven to track the position reference by feedback control. The measurement result of the consumed power of this operation is shown in Fig. 5(b). The primary-side voltage is designed using this measured consumed power in the simulations and experiments.

5.2 Simulation

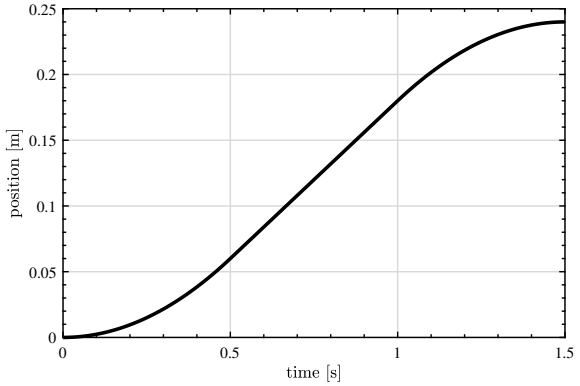

(a) Reference of motion trajectory.

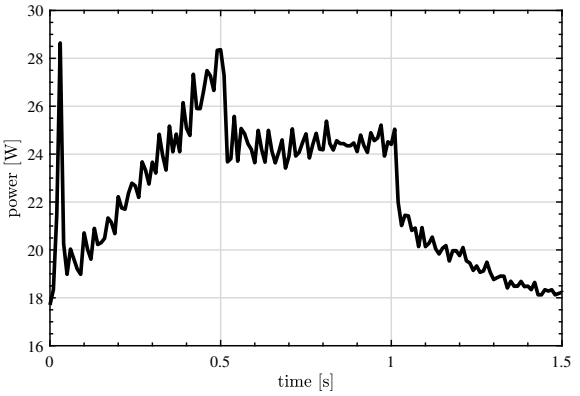

(b) Consumed power.

Fig. 5. Target operation of simulations and experiments.

5.2.1 Condition In the simulations, the following methods are compared.

(1) Optimal voltage ratio method;
$A_{\mathrm{v}} = A_{\mathrm{vopt}}$.

(2) Constant rectification ratio method;
$r_\alpha(t) = 0.3, 0.4, 0.5, 0.6, 0.7, 0.8$.

(3) Proposed optimal rectification ratio method;
$r_\alpha(t) = \alpha_{\mathrm{opt}}(t)$.

The short-mode loss reduction method, i.e., $r_\alpha(t) = 1$, is not compared because this method results in instability of the WPT system in the experiments due to the transmission power shortage. Instead, the constant rectification ratio methods with $r_\alpha(t) = 0.3, 0.4, 0.5, 0.6, 0.7, 0.8$ are simulated for comparison.

In the simulations, the secondary-side DC voltage V_{L} is assumed to be fixed at 25 V. The primary-side voltage V_1 is calculated as (8) in the optimal voltage ratio method. On the other hand, V_1 is derived from (21) with the reference of the rectification ratio r_α and the load power P_{L}. Then, the primary-side DC voltage V_{in} is calculated as

$$V_{\mathrm{in}} = \frac{\pi}{2\sqrt{2}} V_1. \quad \cdots\cdots (26)$$

5.2.2 Result The simulation results are presented in Fig. 6. Fig. 6(a) and Fig. 6(b) show the primary-side DC voltage V_{in}. Fig. 6(c) and Fig. 6(d) present the AC-AC power transmission efficiency η_{ac} which is calculated by (6). Fig. 6(e) and Fig. 6(f) show the rectification ratio α derived from (20). Fig. 6(g) and Fig. 6(h) present the average transmission power $\overline{P}_1$ given by (22). Fig. 6(i) shows the total

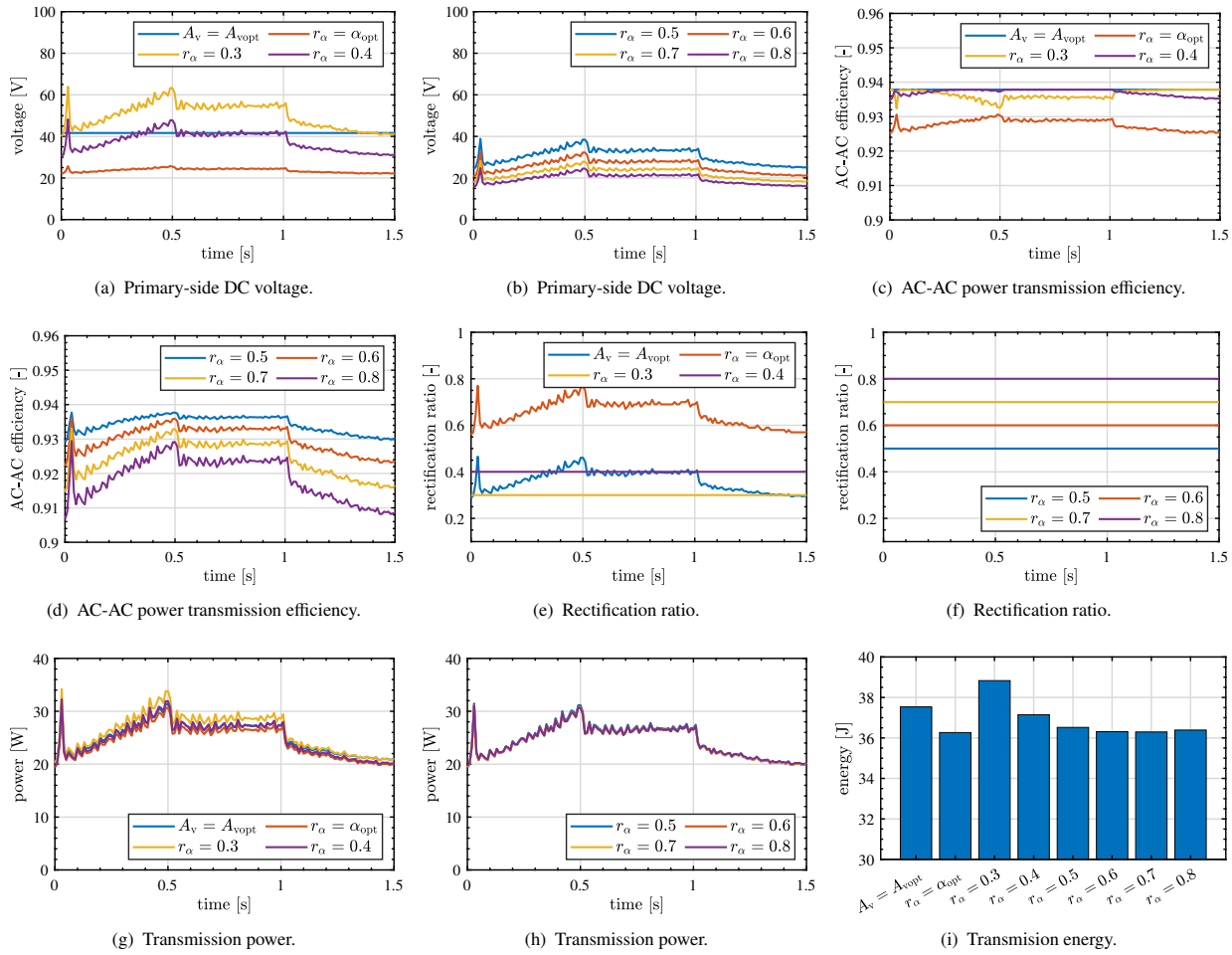

(a) Primary-side DC voltage. (b) Primary-side DC voltage. (c) AC-AC power transmission efficiency.

(d) AC-AC power transmission efficiency. (e) Rectification ratio. (f) Rectification ratio.

(g) Transmission power. (h) Transmission power. (i) Transmision energy.

Fig. 6. Simulation results.

transmission energy calculated by time integral of $\overline{P}_1$.

The optimal voltage ratio method achieves the highest AC-AC power transmission efficiency. The total transmission energy, however, is not the smallest due to the low rectification ratio. The proposed approach results in the lowest transmission energy, and thus the proposed approach can contribute to the high-efficiency operation of WHPS.

5.3 Experiment

5.3.1 Condition The same methods as in the simulations are verified in the experiments with WHPS. In the experiments, the two-mode control method stabilizes the secondary-side DC voltage around 25 V. In each method, the secondary-side DC voltage is assumed to be 25 V, and then the primary-side DC voltage is calculated. The primary-side DC voltage is controlled in the power source to track the calculated value.

5.3.2 Result The experimental results are presented in Fig. 7. Fig. 7(a) and Fig. 7(b) show the measured primary-side DC voltage V_{in}. Fig. 7(c) and Fig. 7(d) present the primary-side DC voltage filtered with the zero-phase low-pass filter (LPF) whose cutoff frequency is 50 Hz. Fig. 7(e) and Fig. 7(f) show the measured rectification ratio α. According to these figures, the rectification ratio almost tracks its reference. Fig. 7(g) and Fig. 7(h) present the input power $\overline{P}_1$ averaged over one cycle of the two-mode control. Here, the power is calculated by measuring the inverter voltage and current. Fig. 7(i) shows the total input energy from the inverter calculated by the time integral of $\overline{P}_1$. The experiments are repeated five times under the same conditions to handle the input energy statistically. The bar charts denote the average energy of the five experiments, and the error bars show the highest and lowest energy.

Similar to the simulation results, the proposed approach achieves the lowest input energy. The effectiveness of the proposed approach is verified through simulations and experiments.

Note that, according to Fig. 6(i) and Fig. 7(i), the constant rectification ratio method with $r_\alpha(t) = 0.6$ shows results similar to the proposed approach. This indicates that the primary-side voltage design based on the rectification ratio may be more useful than the optimal voltage ratio method if the WPT system is under the two-mode control.

6. Conclusion

In this paper, the high-efficiency operation method of WHPS by primary-side voltage control is developed. In the developed method, the secondary-side rectification ratio is used to design the primary-side voltage. The effectiveness of the method is verified through the simulations and experiments.

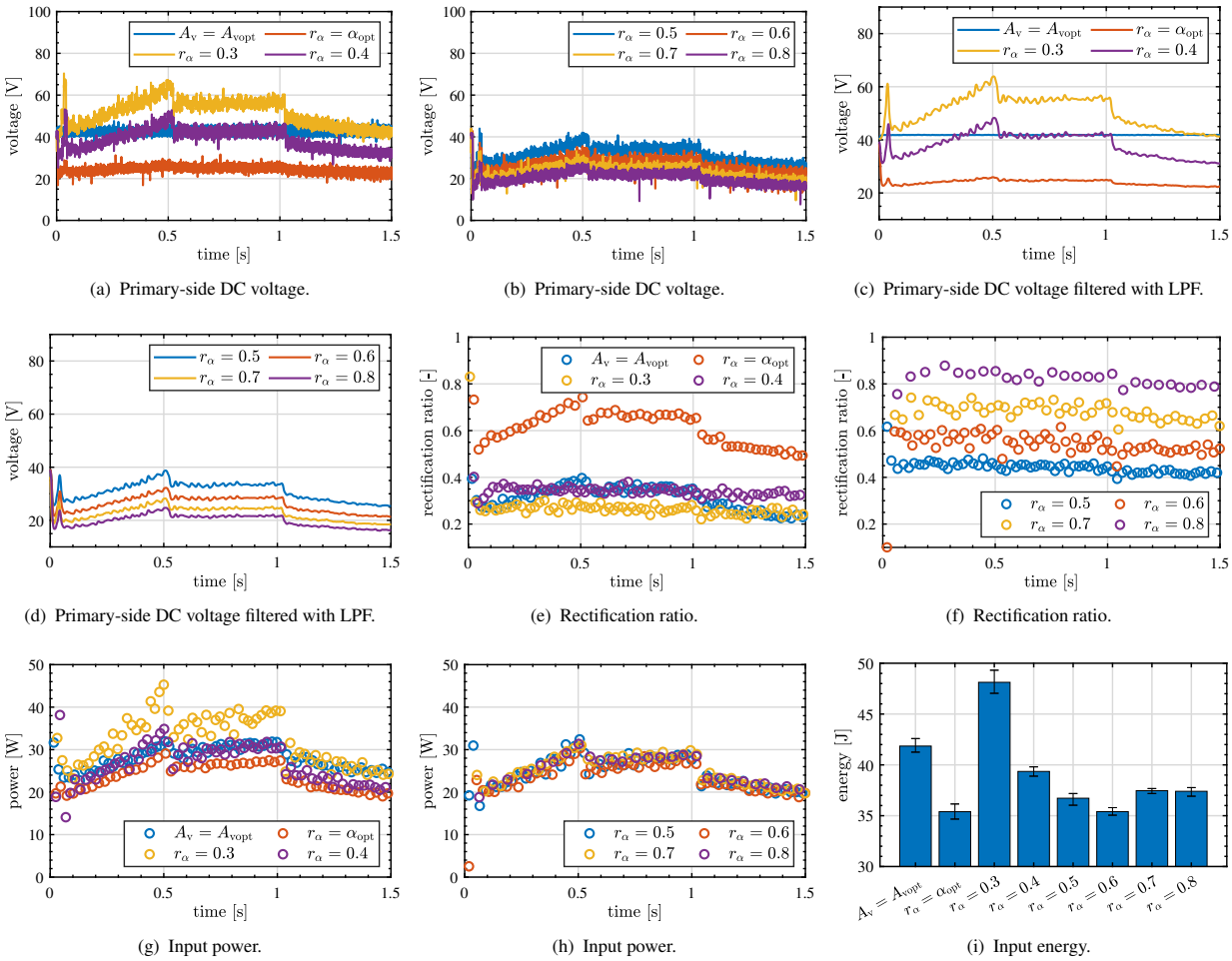

(a) Primary-side DC voltage. (b) Primary-side DC voltage. (c) Primary-side DC voltage filtered with LPF.

(d) Primary-side DC voltage filtered with LPF. (e) Rectification ratio. (f) Rectification ratio.

(g) Input power. (h) Input power. (i) Input energy.

Fig. 7. Experimental results.

References

(1) K. Saiki, A. Hara, K. Sakata, and H. Fujimoto, "A Study on High-Speed and High-Precision Tracking Control of Large-Scale Stage Using Perfect Tracking Control Method Based on Multirate Feedforward Control," *IEEE Trans. Ind. Electron.*, vol. 57, no. 4, pp. 1393–1400, 2010.

(2) J. van Zundert and T. Oomen, "On inversion-based approaches for feedforward and ILC," *Mechatronics*, vol. 50, pp. 282–291, 2018.

(3) M. Mae, W. Ohnishi, H. Fujimoto, K. Sakata, and A. Hara, "Frequency response data-based peak filter design applied to MIMO large-scale high-precision scan stage," *Mechatronics*, vol. 83, no. October 2021, p. 102733, 2022.

(4) Y. Yazaki, H. Fujimoto, K. Sakata, A. Hara, and K. Saiki, "Settling time shortening method using final state control for high-precision stage with decouplable structure of fine and coarse parts," in *IECON 2014 - 40th Annu. Conf. IEEE Ind. Electron. Soc.*, vol. 135, no. 3. IEEE, 2014, pp. 2859–2865.

(5) R. van Herpen, T. Oomen, E. Kikken, M. van de Wal, W. Aangenent, and M. Steinbuch, "Exploiting additional actuators and sensors for nano-positioning robust motion control," *Mechatronics*, vol. 24, no. 6, pp. 619–631, 2014.

(6) T. Oomen, "Advanced Motion Control for Precision Mechatronics: Control, Identification, and Learning of Complex Systems," *IEEJ J. Ind. Appl.*, vol. 7, no. 2, pp. 127–140, 2018.

(7) W. Ohnishi, H. Fujimoto, and K. Sakata, "Model-based Control Techniques for Large-Scale High-Precision Stage," *IEEJ Trans. Ind. Appl.*, vol. 140, no. 4, pp. 272–280, 2020.

(8) M. Steinbuch, T. Oomen, and H. Vermeulen, "Motion Control, Mechatronics Design, and Moore's Law," *IEEJ J. Ind. Appl.*, vol. 11, no. 2, pp. 245–255, 2022.

(9) Y. Yazaki, W. Ohnishi, T. Imura, H. Fujimoto, K. Sakata, A. Hara, Z. Chen, K. Yokovama, and K. Suzuki, "Development of Multi-Axis High-Precision Stage Using Multistep Wireless Power Transfer," in *IECON 2018 - 44th Annu. Conf. IEEE Ind. Electron. Soc.*, vol. 2. IEEE, 2018, pp. 4799–4804.

(10) Y. Yazaki, W. Ohnishi, T. Imura, H. Fujimoto, K. Sakata, A. Hara, Z. Chen, K. Yokoyama, and K. Suzuki, "Evaluation of Disturbance Caused by Cable Tension in Multi-axis High-Precision Stage using Wireless Power Transfer," in *5th IEEJ Int. Work. Sensing, Actuation, Motion Control. Optim.*, 2019.

(11) Y. Fujishima, S. Ishiyama, S. Isago, A. Fukui, H. Yamamoto, T. Hirayama, T. Matsuyama, and Y. Ohmura, "Comprehensive thermal aberration and distortion control of lithographic lenses for accurate overlay," in *Opt. Microlithogr. XXVI*, W. Conley, Ed., vol. 8683, no. April 2013, 2013, p. 86831I.

(12) M. Kato, T. Imura, and Y. Hori, "Study on maximize efficiency by secondary side control using DC-DC converter in wireless power transfer via magnetic resonant coupling," in *2013 World Electr. Veh. Symp. Exhib.*, vol. 6, no. 4. IEEE, 2013, pp. 1–5.

(13) R. Katada, Y. Yazaki, T. Imura, H. Fujimoto, K. Sakata, A. Hara, Z. Chen, K. Yokoyama, K. Suzuki, and Y. Yazaki, "Input Voltage Control Scheme for High Efficiency Operation of Multi-axis High-Precision Wireless Powered Stage," in *5th IEEJ Int. Work. Sensing, Actuation, Motion Control. Optim.*, 2019.

(14) D. Gunji, T. Imura, and H. Fujimoto, "Stability analysis of constant power load and load voltage control method for Wireless In-Wheel Motor," in *2015 9th Int. Conf. Power Electron. ECCE Asia (ICPE-ECCE Asia)*. IEEE, 2015, pp. 1944–1949.